THE INFLUENCE OF MOUNTAINS ON AIRFLOW

Akira WATANABE*

Abstract We have considered the influence of the mountainous region in Central Japan on airflow by the use of meteorological elements, mean dynamical quantities and their spectrum. It has been shown that the foehn phenomenon appears on the lee side of the mountains, the friction velocity is larger on the lee side than on the windward side, and the geopotential height, temperature and eastward component wind spectrum in the upper layer on the lee side agree with those on the windward side over short periods. The mixing ratio spectrum on the 850 mb isobaric surface on the lee side is leess than that on the windward side. The variation of divergence on the lee side is larger than that on the windward side.

1. Introduction

It is well known that there are different effects of orography on airflows: for example, on the planetary scale, airflow over mountains is affected by the earth's curvature and rotation which set up horizontal wave motion, while, on the synoptic scale, cyclogenesis is most frequent in the lee of large mountain barriers. On the meso-scale, a train of lee waves is set up on the lee side of mountain barriers. The effects of orography on airflows are different for different scales of air motion. The planetary scale effects of an orographic barrier on an airflow crossing it are usually explained by the equation for the conservation of potential vorticity (Bolin, 1950). The synoptic scale effect of cyclogenesis was reported by Reitan (1974) based on the data for January, April, June, July and October from 1951–1970 over North America. Scorer (1949) and Sawyer (1960) have studied lee wave which are related to the mean horizontal component perpendicular to the barrier and are inversely proportional to stability. There are many investigation of the effect of mountains on airflow has been investigated by numerical simulation, but there are not only investigations from analytical point of view that Lyons and Murakami (1981) and Murakami (1981a, b) has investigated the effects of the Rocky Mountains and Tibet Plateau on airflow. The purpose of this paper is to consider the influence of the mountains of Central Japan on airflow from an analytical point of view. In particular, we consider the differences between different regions, and the scale on which difference of each element are significant.

* Department of Earth Science, Faculty of Education, Fukushima University.

2. Data and Analytical Method

The data for the analysis used here are 12 hourly upper air records in 1975, observed by the Japan Meteorological Agency at four meteorological stations, Wajima (600), Tateno (646), Hachijojima (687) and Hamamatsu (681), shown in Figure 1. We have analyzed the four elements geopotential height, temperature, humidity, and wind on the each isobaric surfaces 1000mb, 850mb, 700mb, 500mb. We have calculated the mean values, standard deviations, regression coefficients and constants of linear trend from these data. Furthermore, we have calculated the dynamical quantities in the mountainous region (600-646-681) and the lee side region (646-681-687) shown in Figure 1 by Watanabe's method (1981, 1982).
Divergence D is expressed by

$$D = \frac{\partial U}{\partial x} + \frac{\partial V}{\partial y} \quad \cdots\cdots (1)$$

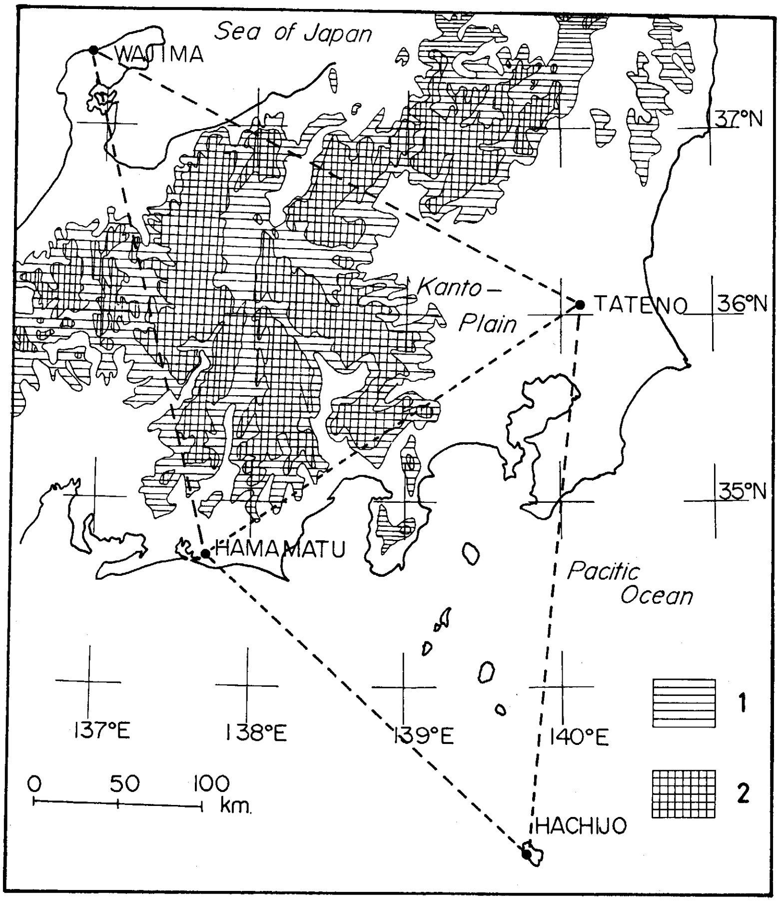

Fig. 1 Topographic map of Central Japan and the computed area. The station locations are indicated by solid circles.
1: area over 500m, 2: area over 1000m. Triangular nets indicate areas in which physical quantities were examined.

Vorticity ζ is expressed by

$$\zeta = \frac{\partial V}{\partial x} - \frac{\partial U}{\partial y} \quad \cdots\cdots (2)$$

Advection temperature A_t is expressed by

$$A_t = U\frac{\partial T}{\partial x} + V\frac{\partial T}{\partial y} \quad \cdots\cdots (3)$$

Advection mixing ratio A_q is expressed by

$$A_q = U\frac{\partial q}{\partial x} + V\frac{\partial q}{\partial y} \quad \cdots\cdots (4)$$

where U, V are the eastward and northward components of wind, respectively, T is the temperature and q is the mixing ratio. We will discuss the different vertical profiles in each region. We have used the data, after removing linear trends, for the Fourier analysis of each meteorological element at each stations and each dynamical quantity in each region. Hence, each data time series F(t) is expressed by

$$F(t) = \sum_{i=1}^{N/2} \alpha_i \cos \omega it + \sum_{i=1}^{N/2} \beta_i \mathrm{Sin}\, \omega it \quad \cdots\cdots (5)$$

where N is the number of data (730). The amplitude spectrum (hereinafter referred to as spectrum) C_n is defined by

$$C_n = \alpha_n^2 + \beta_n^2 \quad \cdots\cdots (6)$$

We will consider the different spectra in each station and region.

3. Vertical Distribution of Mean Values

Vertical distribution of mean meteorological elements

The mean values of geopotential height, temperature and relative humidity at each station and in each region are shown in Table 1. There is a large difference between east and west stations on the 1000mb isobaric surface; the east side has relatively low geopotential height, while the west side is relatively high. In contrast, there is a large difference between north and south stations on the 850mb isobaric surface. The north side shows relatively low temperature and the south side relatively high temperature; in particular Hamamatsu shows a very high temperature. A high correlation (correlation coefficient 0.91–0.99) exists between geopotential height and temperature except on the 1000mb isobaric surface. High relative humidity exists at Wajima dependent upon the low temperature, except on the 850mb isobaric surface. A high negative correlation exists between relative humidity and temperature on the 700mb (–0.99) and 1000mb (–0.68) isobaric surfaces, but the other isobaric surfaces do not show a significant correlation coefficient. In particular, the relative humidity on the 850mb isobaric surface at Tateno is lower than that at Hamamatsu and Hachijojima, while the temperature on the same surface at Tateno is lower than that at the other stations.

Table 1 Mean values of geopotential height, temperature and relative humidity.

Isobaric surface	Station	Geopotential height (m)	Temperature (°C)	Relative humidity (%)
1000 mb	600	131.42	12.3	78.1
	646	126.16	12.5	77.3
	681	130.20	17.1	77.1
	678	123.40	14.3	77.3
850 mb	600	1477.19	4.8	75.8
	646	1478.27	6.3	68.8
	681	1498.93	8.9	77.3
	678	1481.52	7.0	77.3
700 mb	600	3038.39	− 3.3	59.6
	646	3049.06	− 1.7	55.7
	681	3086.44	1.7	50.7
	678	3057.65	− 0.3	54.5
500 mb	600	5630.04	−17.4	44.4
	646	5662.67	−15.6	42.2
	681	5729.71	−12.4	42.8
	678	5683.85	−14.1	45.1

The mixing ratio at Tateno is 4.8g/kg, the same as at Wajima.

The height of the isentropic surface is calculated from the geopotential height and temperature. The results are shown in Table 2. The height of equivalent potential temperature at Wajima is higher on every surface than at the other stations. As the thickness between equivalent potential temperature surfaces at Wajima is thinner at higher potential temperature, while at Tateno this relation is reversed. From this fact it is indicated that at relative lower layer a large gradient of potential temperature exists, and the equivalent potential temperature surface is descending toward Tateno.

Table 3 shows the thickness and the deviation of temperature between several isobaric surfaces. The thicknesses at Wajima, particularly at relatively low temperature, are thinner than at the other stations. The temperature deviation at Tateno is smallest between the 1000mb and 850mb isobaric surfaces. As stated above, the thickness between equivalent potential temperature surfaces is thinnest at Tateno. It appears that the potential temperture surface goes down around the 850mb isobaric surface; this may be caused by the heating due to adiabatic compression. The thickness of between 1000mb and 850mb is thick due to expansion. The deviation of temperature between 1000mb and 850mb is small, apparently due to the heating around the 850mb level. It is relevantly pointed out that the

Table 2 Isentropic surface height (g.p.m).

Station	285°K	290°K	295°K	300°K
600	25.1	1181.2	2224.6	3229.3
646	2.0	942.3	1901.5	2885.7
681	−1223.0	63.3	1349.7	2276.8
678	− 422.5	687.1	1735.9	2631.4

Table 3 Thickness (g.p.m/mb) and temperature deviation (°C/100g.p.m).

Station	1000–850mb	850–700mb	700–500mb
600	8.97 (0.56)	10.41 (0.52)	12.96 (0.54)
646	9.01 (0.46)	10.47 (0.51)	13.07 (0.53)
681	9.12 (0.60)	10.58 (0.46)	13.22 (0.53)
678	9.05 (0.54)	10.51 (0.46)	13.13 (0.53)

foehn phenomenon occurs in the Kanto Plain, whereas Yoshino (1976) indicated that the Bora phenomenon occurs in the same region.

Figure 2 shows the vertical profile of wind velocity. Figure 2a shows the vertical profile of the eastward component (U) of wind which was calculated from the vector average. The vertical profile of the U-component varies linearly with pressure and altitude on the log scale. We take advantage of the logarithmic height dependence of the vertical wind profile in the boundary layer to express the wind velocity U(z) at altitude z

$$U(z) = \frac{U_*}{k} \ln \frac{z}{z_o} \quad \cdots\cdots (7)$$

where U* is the friction velocity, z is the roughness, and k is the von Karman constant (0.4). Meanwhile, we can express the linear regression equation by the method of least squares.

$$\ln z = aU(z) + b \quad \cdots\cdots (8)$$

Comparing equations (7) and (8), we obtain

$$U_* = \frac{k}{a}, \quad \ln z_o = b \quad \cdots\cdots (9)$$

Roughness and friction velocity are obtained from equation (9). The results are shown in Table 4. These values are relatively large at Tateno on the lee side. It appears that severe turbulence occurs in this region.

The vertical distribution of the northward components (V) is shown in Figure 2b. These

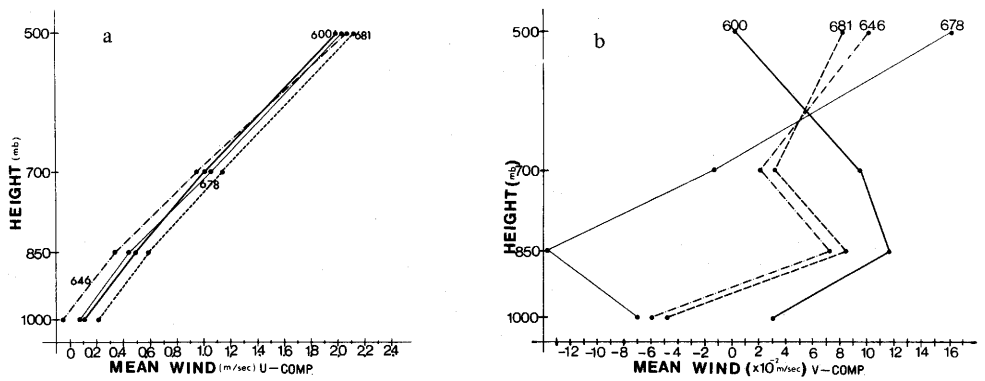

Fig. 2 Vertical distribution of mean wind speed.
a: eastward component of wind. b: northward component of wind.

Table 4 Roughness and friction velocity of synoptic scale (Eastward component of wind).

Station	Roughness (m)	Friction velocity (m/s)
600	279	0.529
646	379	0.602
681	241	0.536
678	293	0.551

are very different from U-components, but the absolute difference is small. Hence, we can say that the region concerned is in the westerly wind field with mean values.

As a result, it was made clear that the foehn phenomenon occurs in the Kanto Plain and the friction velocity is large on the lee side.

Vertical distribution of mean values of dynamical quantities

Figure 3 shows the vertical distribution of mean divergence in the mountainous region and on the lee side. The values of divergence are large in the lee side region except on the 850mb isobaric surface. In particular, the largest value of convergence is on the 1000mb isobaric surface. The variation of divergence is large at about the summit altitude of the mountains, and the divergence itself is larger at the layer lower than the mountain summit, as seen in the standard deviation of divergence in the figure.

Figure 4 shows the vertical distribution of mean value of vorticity in the both regions.

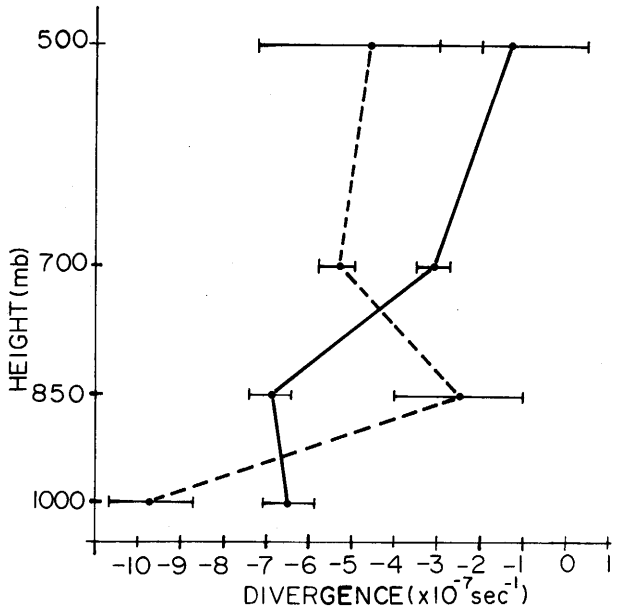

Fig. 3 Vertical distribution of mean divergence.
Solid line: mountainous region. Broken line: lee side region.

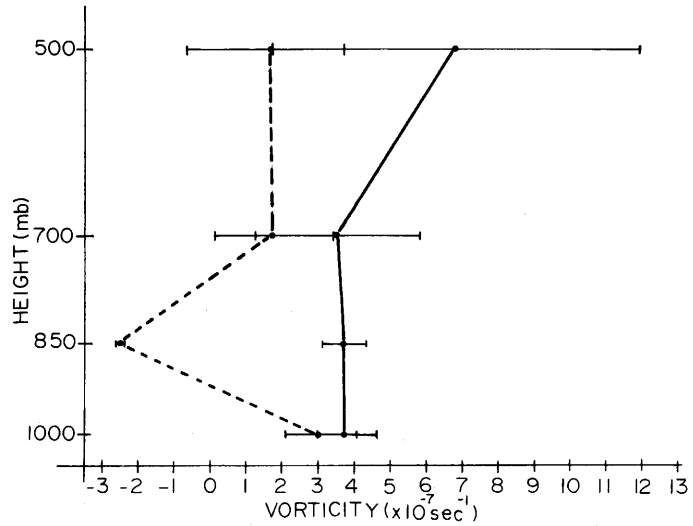

Fig. 4 Vertical distribution of mean quantity of vorticity. Explanation is same as Figure 2.

We can consider that positive vorticity is produced from westerly flow on the lee side, as pointed out by Bolin (1950), but the mean value of vorticity in the mountainous region is larger than that on the lee side on every isobaric surface. Negative vorticity appears on the lee side on the 850mb isobaric surface, and the variation of the vorticity is small. However, it is possible that the computed area is not consistent with the scale of the mountains.

Figure 5 shows the vertical distribution of mean temperature advection. Negative temperature advection appears in the mountainous region on the 850mb and 1000mb isobaric surfaces; on the contrary, positive temperature advection appears in the lee side region on every isobaric surface. This is resonable, when we consider the presence of a foehn condition.

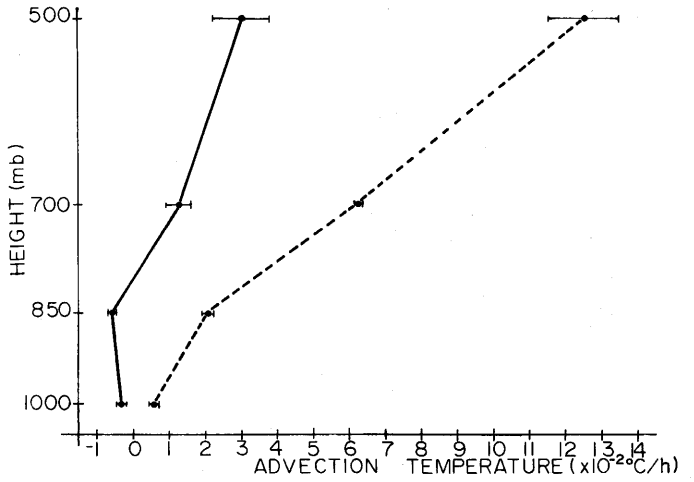

Fig. 5 Vertical distribution of mean temperature advection. Explanation is same as Figure 2.

Figure 6 shows the vertical distribution of mean mixing ratio advection. Positive mixing ratio advection appears in the lee side region on every isobaric surface except 1000mb, and negative mixing ratio advection appears on the 850mb isobaric surface in the mountainous region. Considering the foehn phenomenon, mixing ratio advection should be zero due to dry foehn, or negative due to wet foehn, but the mixing ratio advection seems to be positive. The vertical distribution of mixing ratio advection is caused by a northward wind.

Summarizing the facts stated above, it does not always that positive vorticity appears in the lee side region, the foehn phenomenon occurs in the Kanto Plain, the variation of divergence at the summit level of the mountain is large, and the magnitude of convergence is large in the lower layer (below the mountain height) on the lee side. Positive temperature advection appears in the lee side region.

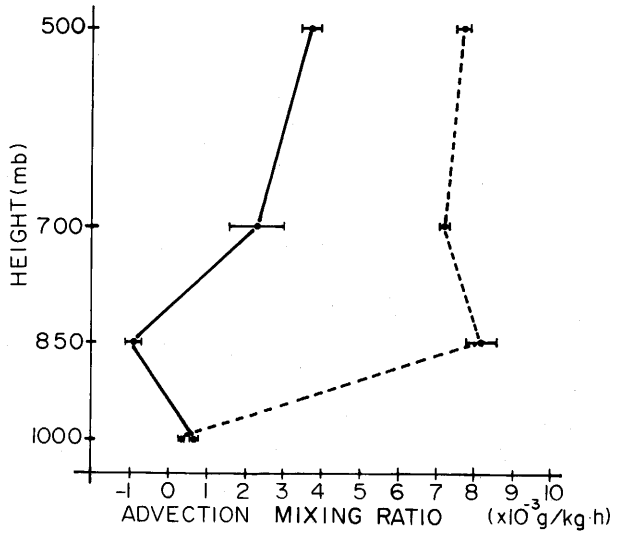

Fig. 6 Vertical distribution of mean mixing ratio advection. Explanation is same as Figure 2.

4. Characteristics of Spectrum Distribution

Spectral distribution of geopotential height on isobaric surface

Figure 7 shows the spectrum of geopotential height on every isobaric surface at Wajima and Tateno from wave numbers 1 to 109. The spectrum decrease a little at upper layer which is called red noise spectrum. Comparing the spectra at Wajima and Tateno, the difference between the stations is large from about wave number 30 (about 12 days period) on the 500mb isobaric surface, from about wave number 15 (about 24 days period) on the 850mb isobaric surface, from about wave number 20 (about 18 days period) on the 700mb isobaric surface and from about wave number 10 (about 36 days period) on the 1000mb isobaric surface.

Namely, the spectrum intensity corresponds to the time scale in the upper layer, but not in the lower layer. There is large deference concerning the spectrum intensity in long period in the lower layer. On an average, the spectrum intensity distinguishes Tateno from the other stations on every isobaric surface, except the 500mb isobaric surface. Furthermore, there is a

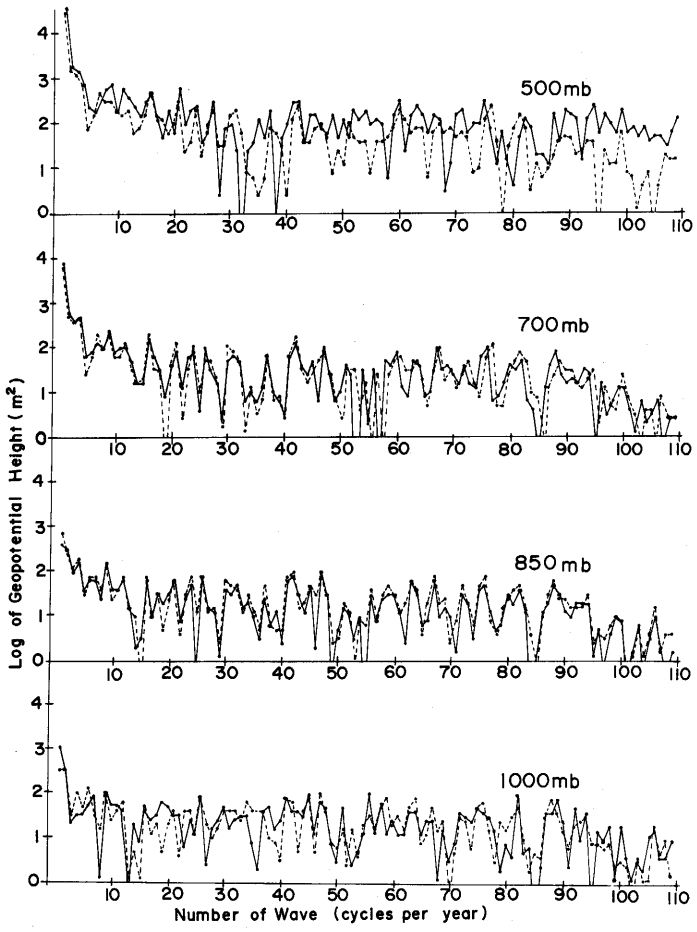

Fig. 7 Distribution of geopotential height spectrum. Solid lines indicate the spectrum at Wajima; broken lines indicate the spectrum at Tateno.

spectral peak from wave number 40 to 48 (about 8 days period) on every isobaric surface except 1000mb, and from wave number about 60 (about 6 days period) to about 95 (about 4 days period) on every isobaric surface except 500mb.

Spectral intensity and its variation are common to both stations with these spectrum peak. There is a spectrum sink with wave number about 53 (about 7 days period) on every isobaric surface except 500mb and with wave number about 15 (about 24 days period) on 850mb and 1000mb isobaric surface.

Distribution of temperature spectrum

Figure 8 shows the temperature spectrum on every isobaric surface at Wajima and Tateno. The spectrum decrease is slight as wave number increases in upper layer, similarly to the geopotential height spectrum. This is called a red noise spectrum. The difference between the spectra at the two stations is small on the 500mb and 700mb isobaric surfaces. There is a large difference from wave number of about 10 to larger wave numbers on the

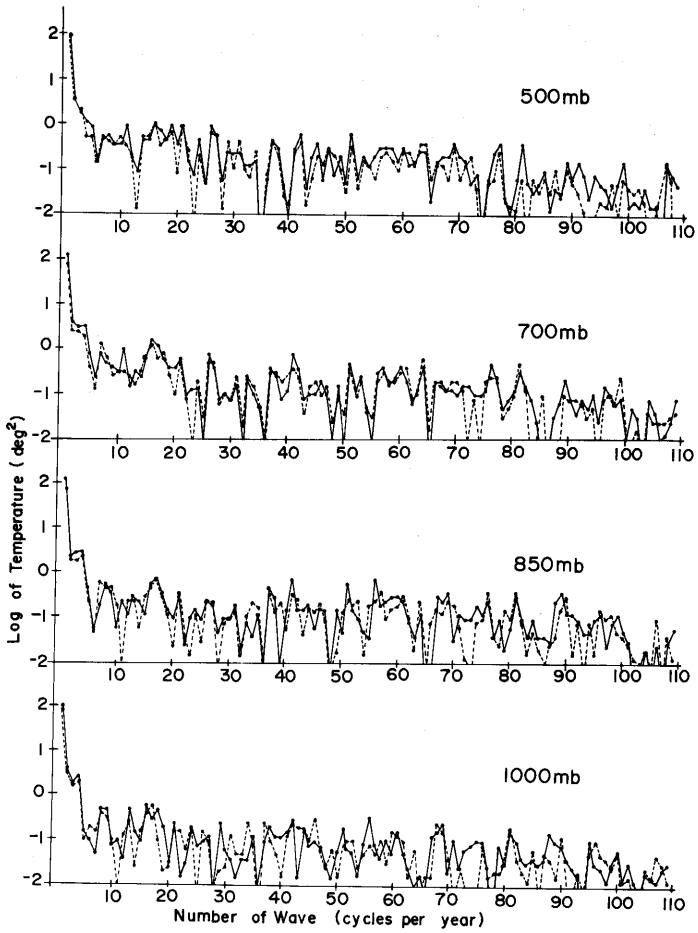

Fig. 8 Distribution of temperature spectrum. Explanation is same as Figure 7.

850mb and 1000mb isobaric surfaces. Especially, the spectrum at Tateno is smaller than that at Wajima on the 850mb isobaric surface. There are spectral peaks around wave number 16 (about 23 days period) and around wave number 60 (about 6 days period) on every isobaric surface at every station. One would expect the positive correlation between the geopotential height and temperature spectra, but the geopotential height spectrum has a minimum around wave number 16 on the 850mb and 1000mb isobaric surfaces. This period was pointed out by Mildner (1930) and Hänsh (1932) as a typical time scale of air mass exchanges and air mass transformations. Around the wave numbers 5 and 6 which are fundamental modes of this period, there is a spectral minimum. Hence, we can consider that this period is a dominant spectrum. The spectral intensity at Tateno is smaller than that at Wajima from about the wave numbers 11 and 22 on the 850mb and 1000mb isobaric surfaces, respectively. In particular, there is a spectral minimum from the wave numbers 20 to 30 on the 850mb isobaric surface at Tateno. The difference of spectrum intensity at both stations is pronounced from the wave number about 80 to larger wave numbers on the 500mb isobaric

surface, and from about wave number 70 to larger wave numbers on the 700mb isobaric surface.

Distribution of wind spectrum

Figure 9 shows the wind spectrum on every isobaric surface. Figure 9a shows the spectra of the U-components at Wajima and Tateno. Figure 9b also shows the spectra of the V-components at Wajima and Hamamatsu. The spectra of U-components show a red noise type spectrum in the upper layer, while the spectra at 850 mb and 1000mb indicate nearly white noise. The spectral intensity is not different on every isobaric surface at both stations, except on 850mb. The spectral intensity at Tateno is smaller than that at Wajima at 850mb level, but the geopotential spectral intensity at Tateno is larger than that at Wajima. The wind spectrum $(\Delta V)^2$ and geopotential height spectrum $(\Delta\Phi)^2$ are related as follows;

$$\Delta P \simeq \rho \Delta\Phi, \quad \Delta P \simeq \rho\,(\Delta V)^2$$

Hence,

$$\Delta\Phi \simeq (\Delta V)^2, \quad (\Delta\Phi)^2 \simeq (\Delta V)^4$$

Namely, the geopotential height spectrum is related to the square of the wind spectrum. This suggests that the effects of orography and friction are large in the lee side region. It appears that there is a larger effect on the 1000mb isobaric surface, but it is not so clear on the 850mb isobaric surface. There are spectral peaks from the wave numbers about 33 (about 11 day period) to 55 (about 7 day period) and at the wave numbers around 75, 85, and 95 (about 4 day period) on every isobaric surface except 1000mb. On the other hand, there are spectral minima around the wave number 30 (about 12 day period) and 60 (about 6 day period). The geopotential height spectrum has a peak about the wave number 60, but the U-component wind spectrum has a minimum. This spectral minimum is clear at Tateno. Hence, it is clear that this wind spectrum variation is not correlated with the gradient pressure field.

The spectrum characteristics of V-component show a white noise type on every isobaric surface at every station. There are relative spectral peaks around the wave number 50 (about 7 day period) and from the wave number around 80 to 90 (about 4 day period); these spectral peaks are especially marked at Wajima. This spectral peak corresponds to the geopotential height spectrum peak, but there is not a peak in the U-component wind spectrum.

Distribution of mixing ratio spectrum

Figure 10 shows the distribution of mixing ratio spectra on every isobaric surface at Wajima and Tateno. The spectrum at Wajima is similar to that at Tateno on the 1000mb isobaric surface. The variation of spectral intensity at Wajima is similar to that at Tateno on the 850mb isobaric surface, but the spectral intensity at Tateno is smaller than that at Wajima on the same isobaric surface. We have recognized that the mixing ratio spectrum does not correspond to the temperature spectrum, but does corresponded to the V-component wind spectrum. The difference of spectral intensity between both stations is large from the wave number about 90 to higher wave numbers. There are spectral peaks around the

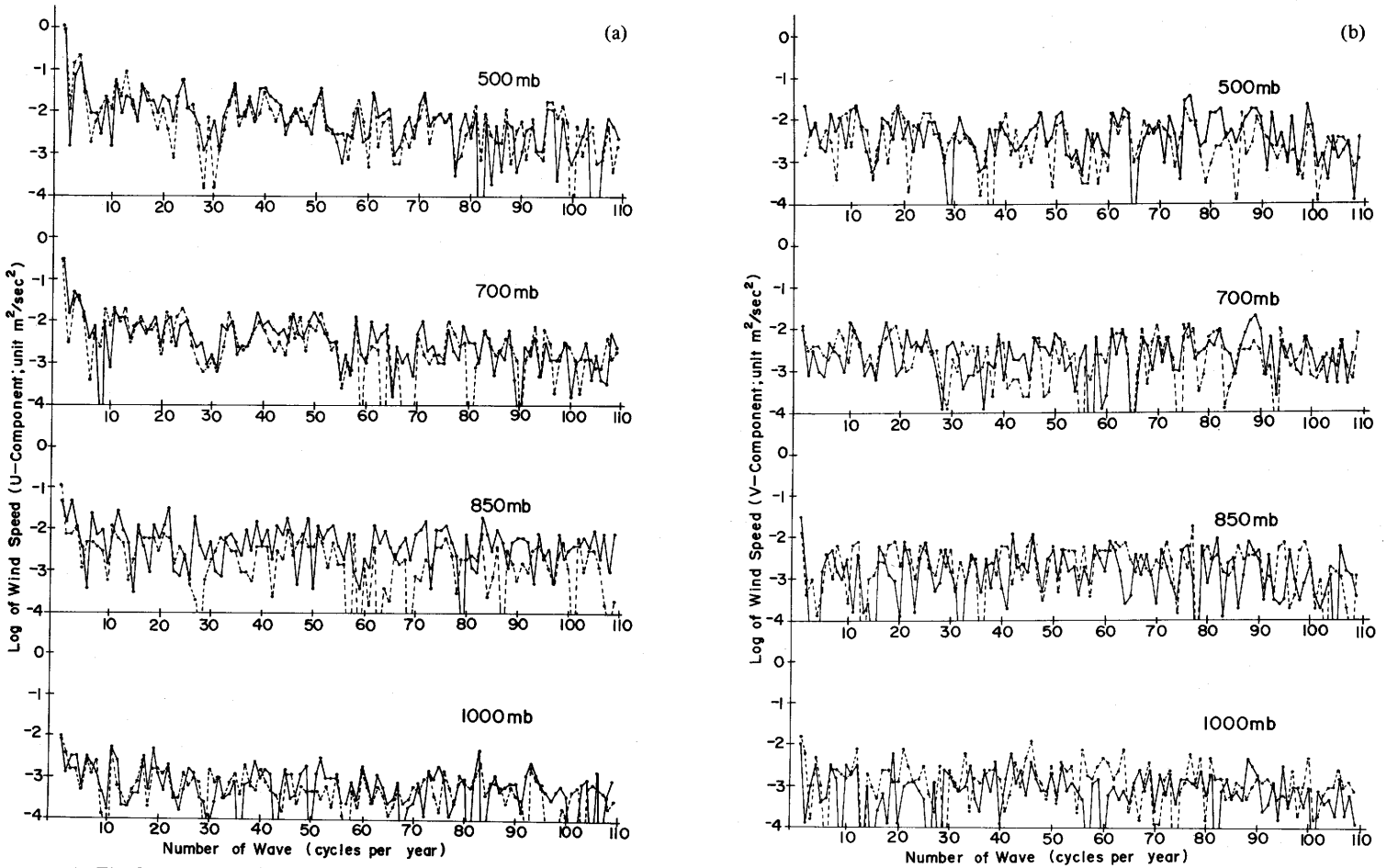

Fig. 9 Distribution of wind spectrum.
a: eastward component of wind. b: northward component of wind. Explanation is same as Figure 7, except broken line of Figure 9b which indicates the spectrum at Hamamatsu.

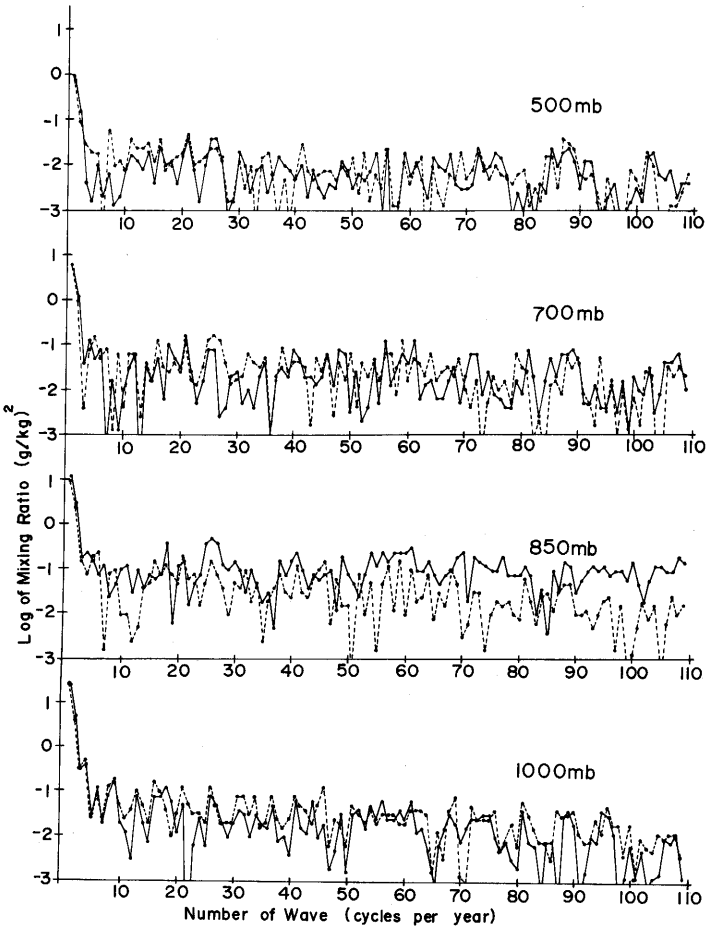

Fig. 10 Distribution of mixing ratio spectrum. Explanation is same as Figure 7.

wave numbers 25 (about 15 day period), 60 (about 6 day period) and 90 (about 4 day period) on every isobaric surface. Though the spectra of meteorological elements on the lee side correlate with those on the windward side in upper layer, only the spectrum of mixing ratio on the lee side correlates with that on the windward side in lower layer. There is no easy physical explanation for these features.

Distribution of divergence spectrum

Figure 11 shows the distribution of divergence in the mountainous and lee side regions. Generally, as the spectra of differential quantities are computed by finite differences, they are not homogeneous in time. A weight dependent on time scale imposes on the spectrum. To simplify matters, we have assumed that the one-dimensional wind distribution u(x) can be approximated by that of the x-component. We obtain

$$u(x) = \frac{1}{\sqrt{2\pi}} \int \Phi(k)\, e^{ikx}\, dk \quad \cdots\cdots\cdots\cdots\cdots\cdots\cdots\cdots\cdots\cdots \quad (10)$$

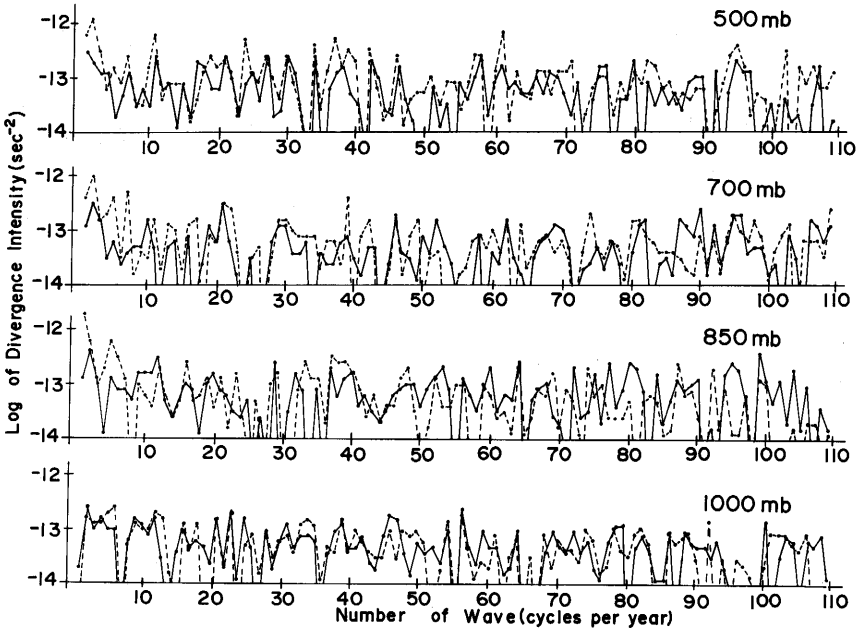

Fig. 11 Distribution of divergence spectrum. Solid lines: mountainous region; broken lines: lee side region.

Hence,

$$\left(\frac{\partial u}{\partial x}\right)^2 = \frac{1}{2\pi}\int k^2 \Phi \Phi^* dk = \frac{<u^2>}{2\pi}\int k^2 F(k)\, dk \quad \cdots\cdots\cdots\cdots\cdots (11)$$

where $|\Phi|^2 = <u^2> F(k)$, k is the wave number and F(k) is the spectrum of u(x). The divergence $(\partial u/\partial x)$ has a spectrum of $k^2 F(k)$. In practice, the divergence was approximated by the finite difference over the finite distance r. The divergence then becomes

$$\frac{u(x+r)-u(x)}{r} = \frac{1}{\sqrt{2\pi}}\int \Phi(k)\, e^{ikx}\left(\frac{e^{ikr}-1}{r}\right) dk \quad \cdots\cdots\cdots\cdots\cdots (12)$$

Hence, the spectrum of divergence is approximately

$$\left\{\frac{u(x+r)-u(x)}{r}\right\}^2 = \frac{<u^2>}{2\pi}\int k^2 F(k)\left(\frac{\sin\frac{kr}{2}}{\frac{kr}{2}}\right)^2 dk \quad \cdots\cdots\cdots\cdots\cdots (13)$$

Namely, the weight of $(\sin\frac{kr}{2} / \frac{kr}{2})^2$ imposes on the spectrum, but here as we have considered the scale of spectrum is larger than r. We can discuss the spectrum in disregard of weight. The divergence spectrum is of the white noise type. The spectra show a slight tendency toward a red noise type on every isobaric surface except 1000mb. This tendency is especially large in the lee side region. The spectral intensity at every wave number is larger than the mean value. Hence, the divergence of the field is determined by the spectrum of each wave number. The spectral intensity in the lee side region is larger than that in the mountainous region at every wave number. This agrees with the formation of a convergence

in the lee side region, which was pointed out by Defant (1951). There are spectral peaks around the wave numbers 20 (about 18 day period), 40 (about 9 day period), 70 (about 5 day period) on every isobaric surface, around the wave number 30 (about 12 day period) except on the 850mb isobaric surface, and around the wave number 95 (about 4 day period) on the 700mb and 500mb isobaric surfaces, while spectral minima occur around the wave numbers 15 (about 24 day period) and 25 (about 14 day period).

The distribution of the vorticity spectrum

Figure 12 shows the distribution of the vorticity spectrum on every isobaric surface in the lee side and mountainous regions. Though the weight as same as divergence impose on the vorticity spectrum, we discuss to same as aforesaid.

The vorticity spectrum is closer to white noise than the divergence spectrum. The spectrum in the mountainous region is larger than that in the lee side region except on the 1000mb isobaric surface. The vorticity spectrum intensity is larger than the mean value at every wave number; hence, the vorticity of the field is determined by the spectrum of each wave number as divergence field. There are spectral peaks around the wave number 90 (about 4 day period) on every isobaric surface, around the wave number 70 (about 5 day period) on the 850mb isobaric surface and around the wave number 15 (about 24 day period), 60 (about 6 day period), and 80 (about 5 day period) on the 500mb isobaric surface. The spectral variation in the lee side region is different from that in the mountainous region except around wave number 70 (about 5 days period) on the 850mb isobaric surface. It is difficult to find the formation of vorticity in the lee side region which was pointed out by Bolin (1950). Though the spectrum in the lee side region is larger than that in the mountainous region on the 1000mb isobaric surface, the vorticity generation is not

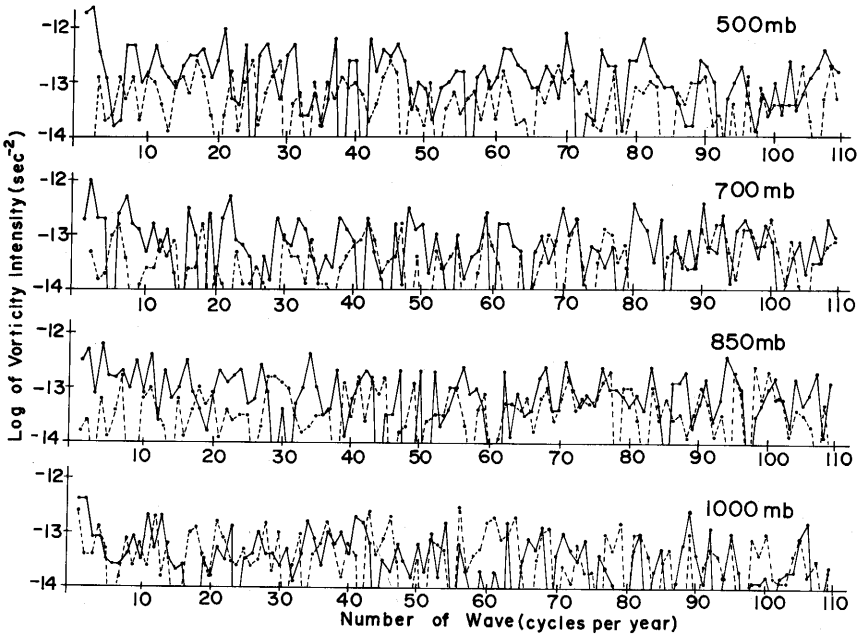

Fig. 12 Distribution of vorticity spectrum. Explanation is same as Figure 11.

due to the conservation of potential vorticity, but due to dynamical effects or effects of friction.

5. Conclusion

We have described the difference of the mean values of meteorological elements and their spectral intensities in the mountainous and lee side regions. The following main results were obtained:

1) It may well be that the foehn phenomenon occurs in the Kanto Plain. 2) The friction velocity of U-component at Wajima is smaller than at the other stations on the lee side, indicating that turbulence is large in the lee side region. 3) The mean value of convergence is large in lower layer in the lee side region, indicating that the convergence is formed by the mountains; but we can not conclude that vorticity is generated in the lee side region. 4) The positive temperature advection in the lee side region is relatively larger than that in the mountainous region. 5) The mixing ratio advection in the lee side region is relatively larger than that in the mountainous region; it is especially large on the 850mb isobaric surface in the lee side region. 6) The geopotential height spectrum in the mountainous region correlates with that in the lee side region for shorter periods (around the wave number 30) in the upper layer, but the spectrum in the mountainous region correlates with that in the lee side region for a long period (around the wave number 10) in lower layer. 7) Though the distribution of temperature spectra shows the same variation on the 700mb and 500mb isobaric surfaces in both regions, the spectra are clearly different on the 1000mb and 850mb isobaric surfaces from around the wave number 10. 8) The wind spectrum intensity of the U-component in the lee side region is smaller than that in the mountains region on the 850mb isobaric surface, indicating that the turbulence is large in the lee side region. Such features are not seen in the geopotential height spectrum. 9) The mixing ratio spectrum intensity in the lee side region is relatively smaller than that in the mountainous region on the 850mb isobaric surface. 10) The divergence spectral intensity is larger than the mean value of the divergence, and the spectral intensity in the lee side region is larger than that in the mountainous region. The vorticity spectrum intensity in the lee side region is smaller than that in the mountainous region except on the 1000mb isobaric surface. It is sure that the vorticity is not formed due to the conservation of potential vorticity, but is to be generated by orographic friction on the 1000mb isobaric surface.

It remains unclear whether all of the aforesaid characteristics are due to the influence of the mountains region of Central Japan. Furthermore, the study of the influence of basic flow pattern is needed.

Acknowledgements

The author wishes to express his thanks to Professor Dr. Ikuo Maejima and Associate Professor Dr. Michio Nogami of Tokyo Metropolitan University for their advice and encouragement throughout this study. Further, the author appreciates valuable discussions

on the subject by the staff of the Climatological Laboratory of Tokyo Metropolitan University.

References Cited

Bolin, B. (1950): On the influence of the earth's orography on the character of the westerlies, *Tellus*, **2**, 184–195.

Defant, F. (1951): Local winds. *Compendium of Meteorology*, 655–672.

Hänsh, F. (1932): Über die 24 Tägige Welle des Winters 1923/24, *Veröff. Geophys. d.: Univ., Leipzig*, **5**, 173–208.

Lyons, S. W., Murakami, T. (1981): Orographic influence of the Rocky Mountains on the winter circulation over the Contiguous United States, Part I. Large-scale aspects, *J. Meteor. Soc. Japan*, **59**, 320–335.

Mildner, P. (1930): Über die Korrelation Zwischen harmonischen Konstituenten und Beobachtungs Kurven mit Anwendungen auf die Luftdruckwellen des Winter 1923/24, *Beiträge zur Physik der freien Atmosphäre*, **14**, 252–262.

Murakami, T. (1981a): Orographic influence of Tibetan Plateau on the Asiatic winter monsoon circulation, Part III. Short-period oscillations, *J. Meteor. Soc. Japan*, **59**, 173–200.

(1981b): Orographic influence of Tibetan Plateau on the Asiatic winter monsoon circulation, Part IV. Long-period oscillations, *J. Meteor. Soc. Japan*, **59**, 201–219.

Reitan, C. H. (1974): Frequencies of cyclones and cyclogenesis for North America, 1951–1970, *Mon. Wea. Rev.*, **102**, 861–868.

Sawyer, J. S. (1960): Numerical calculation of the displacements of a stratified airstream crossing a ridge of small height, *Quart. J. Roy. Meteor. Soc.*, **86**, 326–345.

Scorer, R. S. (1949): Theory of waves in lee of mountains, *Quart. J. Roy. Meteor. Soc.*, **75**, 41–56.

Watanabe, A. (1981): Study of mean field of dynamical quantity in Kanto district*, *Tenki*, **28**, 145–158.

(1982): Seasonal characteristics in mean fields of dynamical quantities*, *Tenki*, **29**, 611–623.

Yoshino, M. M. (1976): Oroshi; ein starker Lokalwind in der Kanto Ebene, Japan, In Yoshino, M. M. (ed.): *Local Wind Bora*, Tokyo University Press, Tokyo, 215–232.

(*in Japanese)